Nonclassical noise features in a correlation plenoptic imaging setup

International Journal of Quantum Information

Non-classical noise features in a Correlation Plenoptic Imaging setup

Emiliana De Scisciolo
Dipartimento Interateneo di Fisica, Università degli studi di Bari, I-70126 Bari, Italy

Francesco Di Lena
Dipartimento Interateneo di Fisica, Università degli studi di Bari, I-70126 Bari, Italy
INFN, Sezione di Bari, I-70126 Bari, Italy

Alessio Scagliola
Dipartimento Interateneo di Fisica, Università degli studi di Bari, I-70126 Bari, Italy

Augusto Garuccio, Francesco V. Pepe
Dipartimento Interateneo di Fisica, Università degli studi di Bari, I-70126 Bari, Italy
INFN, Sezione di Bari, I-70126 Bari, Italy

Alessio Avella, Ivano Ruo-Berchera
Istituto Nazionale di Ricerca Metrologica (INRIM), Strada delle Cacce 91, I-10135 Torino, Italy

Milena D'Angelo
Dipartimento Interateneo di Fisica, Università degli studi di Bari, I-70126 Bari, Italy
INFN, Sezione di Bari, I-70126 Bari, Italy
Istituto Nazionale di Ottica (INO-CNR), I-50125 Firenze, Italy

Sub-shot-noise imaging and correlation plenoptic imaging are two quantum imaging techniques that enable to overcome different problems of classical imaging systems. Combining the two techniques is not trivial, since the former is based on the detection of identical corresponding modes to subtract noise, while the latter requires the detection of different modes to perform directional reconstruction. In this paper, we experimentally show the possibility to obtain a noise-reduction factor smaller than one, a necessary condition to perform sub-shot-noise imaging, in a setup that can be adapted to correlation plenoptic imaging.

1. Introduction

Quantum properties of light and quantum-inspired measurement protocols have recently fostered the development of intriguing technologies in the context of quantum imaging, whose capabilities go beyond those of classical imaging and intreferometry systems, at least in specific tasks.[1,2,3,4,5,6,7,8,9,10,11] In particular, it was discovered that exploiting the photon number correlation between two entangled photon beams, typically emitted by spontaneous parametric down-conversion (SPDC), can provide the possibility to perform sub-shot-noise (SSN)

imaging[12,13] and microscopy[14] of low-absorbing samples. On the other hand, in the context of techniques based on intensity correlation measurements, such as HBT interferometry[15,16] and ghost imaging[1,17,18,19], a technique called Correlation Plenoptic Imaging (CPI) was introduced[20,21,22,23], enabling to perform plenoptic imaging (therefore, 3D recostruction and refocusing) with diffraction limited resolution[24].

Even if it would be beneficial to join the advantages of SSN imaging and CPI, this has not been performed up to now, despite CPI schemes based on SPDC entangled photon pairs have already been proposed[21]. In fact, the SSN imaging protocol is based on the spatial detection of two very similar noise patterns, while in CPI the detected patterns are different, since the two detectors capture the light distributions on the object plane and on the focusing element, which can be very distant from each other.

In this article, we first show an experimental measurement of the noise-reduction factor[12], which is an essential figure of merit to determine the possibility of SSN imaging, in a setup in which SSN imaging, standard imaging and ghost imaging can be performed at the same time. Then, we alter the initial setup by introducing asymmetry between the optical paths followed by the two entangled beams; such setup would enable to perform CPI, provided a specific algorithm to detect the direction of light were developed. We will demonstrate that, despite the two paths are made asymmetric, and the two sensors do not detect identical noise patterns, it is still possible to obtain nonclassical values of the noise-reduction factor. This feature opens the possibility to exploit nonclassical noise properties to reduce the SNR in CPI, by combining the use of entangled photons with properly tailored new measurement schemes.

2. General Aspects

SPDC is a quantum phenomenon that allows to generate pairs of entangled photons by the interaction between a "pump" laser beam and a non-linear crystal[25]. Such interaction can convert a laser photon into two photons, conventionally labeled as "signal" and "idler", whose energies (ω_s, ω_i) and momenta $(\boldsymbol{k}_s, \boldsymbol{k}_i)$ are related to those of the pump photon by the conservation laws:

$$\omega_p = \omega_s + \omega_i, \quad \boldsymbol{k}_p = \boldsymbol{k}_s + \boldsymbol{k}_i. \tag{1}$$

The subscript p, s and i stand for pump, signal and idler, respectively. SPDC has been a milestone in the development of quantum imaging, as early as the first quantum imaging experiment was demonstrated by Pittman et al. in 1995[1]. This experiment showed the possibility to obtain a "ghost" image of an object, by detecting coincidences between signal and idler entangled photons, even if no first-order image of the object was formed in the setup.

A wide variety of applications of quantum imaging has been proposed, besides ghost imaging, in order to overcome specific limitations of standard imaging devices.

Some examples are super-resolution using multi-photon entangled systems[10] and sub-shot noise imaging[12]. In particular, sub-shot-noise (SSN) imaging is possible by illuminating a weak absorptive object with the far-field of one of the SPDC correlated beams (say, the signal). The image is retrieved by measuring the intensity pattern in the arm containing the object, and then subtracting the correlated noise pattern measured in the other arm. The reconstructed image is proportional to the aperture function of the object, and the signal to noise ratio is improved because the thermal noise affecting each single beam is cancelled in the subtraction process, due to the quantum correlations between the two beams[26].

The possibility to obtain SSN images is crucially related to the value of the *noise reduction factor* (NRF) [26,13]

$$\sigma = \frac{\langle \Delta^2(\hat{n}_i - \hat{n}_s)\rangle}{\langle \hat{n}_i + \hat{n}_s\rangle} = \frac{\langle \Delta^2 \hat{n}_i\rangle + \langle \Delta^2 \hat{n}_s\rangle - 2\langle \Delta\hat{n}_i \hat{n}_s\rangle}{\langle \hat{n}_i + \hat{n}_s\rangle} \tag{2}$$

given by the ratio between the variance of the difference in the number of photons and the noise of two coherent states of equivalent intensity. The NRF is also a measure of the degree of correlation between the two modes. This quantity is generally equal or larger than 1 for classical systems; only quantum states of light can give values smaller than 1. In particular for SPDC correlated modes it turns out that $\sigma = 1 - \eta$, where η is the global efficiency in detecting correlated photons. The sub-shot-noise imaging scheme shows an improvement with respect to classical measurement, in terms of signal to noise ratio, using a Poissonian source, which is exactly quantified by the factor σ for weakly absorbing samples.

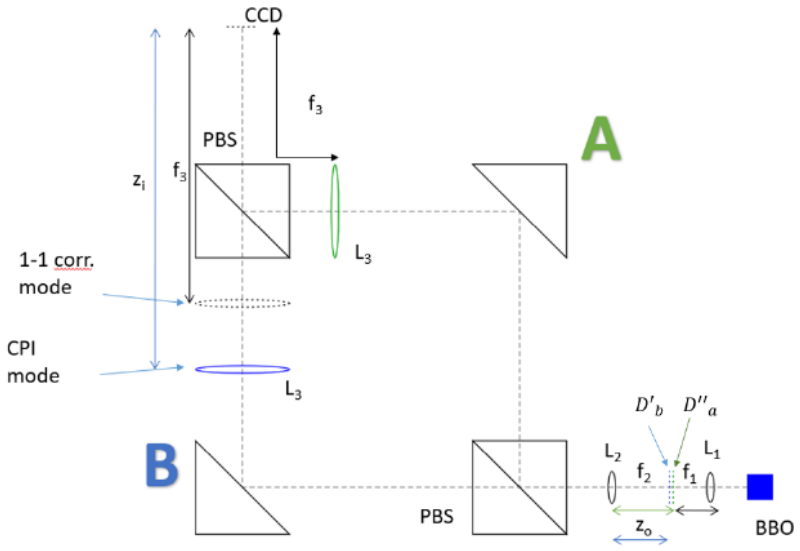

Fig. 1. Schematic representation of the experimental setup employed in the experiment. Details on the components and the parameters are given in the text.

3. Experiment

The experimental setup is shown in Fig. 1. The SPDC source is composed of a single-mode UV laser with wavelength $\lambda = 355\,\text{nm}$ (Genesis CX 355-100 SLM), a half-wave plate and a β-Barium Borate (BBO) crystal ($5\,\text{mm} \times 5\,\text{mm} \times 7\,\text{mm}$, Eksma Optics). The crystal can be rotated in order to obtain type II phase matching condition with beam-like configuration and the half-wave plate can be rotated to align the polarization direction of the pump with the extraordinary direction of the crystal. The two generated beams (signal and idler) pass through a dichroic mirror (not shown in Fig. 1) which reflects the pump, and through the lenses L_1, of focal length $f_1 = 10\,\text{mm}$, and L_2 ($f_2 = 40\,\text{mm}$), before their paths being separated by a Polarizing Beam Splitter (PBS). The distance between L_1 and L_2 is equal to $f_1 + f_2$. Notice that the far field of the SPDC beams is reproduced at a distance f_1 after the lens L_1. The two beams follow similar paths: the reflected beam passes through a fixed lens L_{3A} ($f_3 = 200\,\text{mm}$) then reaches another PBS which reflects it on the CCD sensor (Andor iXon Ultra 897) after passing trough a frequency filter which limits the wavelength range of photons impinging the sensor in the interval $690\,\text{nm} - 730\,\text{nm}$. The transmitted beam passes through a movable lens L_{3B} ($f_3 = 200\,\text{mm}$), the second PBS and the frequency filter, finally impinging on the CCD sensor.

In the "balanced" configuration, the distance between L_2 and both L_{3A} and L_{3B} has been fixed to 200 mm, while the distances between each of the L_3 lenses and the sensor are both equal to f_3. The optical systems composed by the lenses L_2 and $L3_A/L3_B$ is able to map the image of the focal plane of the lens L_1, on which the far field of SPDC is encoded, on the camera plane. In this configuration, if an object is placed in focal plane of L_1, along one of the SPDC beams (say, the signal), its image will be retrieved on the portion of the sensor impinged by the signal far field. Even the idler far field impinges the sensor, and this additional information can be used to first identify corresponding modes and then subtract noise to achieve a SSN image of the object.

In the setup described in Fig. 1, the lens L_{3B} can be moved, in such a way to focus a different plane than the focal plane of L_1 on the sensor. Such configuration, that we will call "unbalanced", can be useful in terms of correlation plenoptic imaging, since now the two lenses L_3 provide images of two different planes, which, after measuring intensity correlations or photon coincidences, could be used to reconstruct the light field between the two planes and perform refocusing and point-of-view changes. However, this situation can be detrimental in terms of SSN imaging, since now the fluctuations of the SPDC beam images formed on the sensor are not (at least ideally) perfectly correlated as in the balanced case. In the following, we will show that a noise-reduction factor smaller than 1 is achievable even in the unbalanced case.

The frequency range is chosen around the degenerate frequency in order to spatially select two distinct spots corresponding to the signal and idler photons.

We also choose propagation configuration in which the two spots are tangent. To compute the NRF, we first had to determine the position of correlated points in the far field of the two SPDC beams. Based on the phase-matching function, such pairs of correlated points are symmetric with respect to the tangency point of the two spots. The spatial correlation matrix is obtained by calculating the NRF between a pixel in the image of one beam and the pixels of a large region in the image of the other (the procedure is presented in greater detail in the following). The pixel in the first beam is then varied to obtain an average correlation matrix. This measurement is also useful to control alignment and focusing of the optical elements.

We expect that correlations are relevant inside the coherence area. The correlation is point-to-point (i.e., a delta function) in case of a plane-wave pump; however in the realistic case of a Gaussian pump, the existence of transverse components of the wave-vector determines a widening of the coherence area. Given a Gaussian pump beam with the waist w at the crystal, the photon correlation function in the focal plane of the lens L_1 is again a Gaussian function (the Fourier transform of the pump) with waist

$$w' = \frac{\sqrt{2}\lambda_{signal} f_1}{\pi w} = 5.36\,\mu\text{m}, \tag{3}$$

where $\lambda_{signal} = 710\,\text{nm}$ refers to the degenerate frequency and $w = 596\,\mu\text{m}$. The FWHM, usually taken as the size of the coherence area in the far field, is

$$\text{FWHM} = 2.355 \times w' = 12.6\,\mu\text{m}. \tag{4}$$

The expected magnification is

$$M_{exp} = -\frac{f_3}{f_2} = 5, \tag{5}$$

while the measured value is slightly different, i.e. $M = 5.32$. Therefore, the coherence length on the sensor is

$$w_0^s = M \times \text{FWHM} = 67\,\mu\text{m}, \tag{6}$$

which is greater than the pixel dimension $\delta_p = 16\,\mu\text{m}$. Thus, the physical pixel is unable to collect all the correlated photons, since most of them fall outside its area. A pixel binning is thus required to optimize the measured correlations.

To pass from the balanced case to the unbalanced one, in which the setup is suitable to perform CPI, we move the lens L_{3B} by 21 mm. Considering such displacement, we obtain that the distance between the focused planes along arms A and B is now $814\,\mu\text{m}$.

The evaluation of NRF is performed by a software which operates as follow:

(1) a pixel P of signal (or idler) spot is chosen;
(2) the symmetric pixel S is found on the other spot;
(3) NRF is calculated between pixel P and each pixel in an area $n \times n$ pixel centered on pixel S;

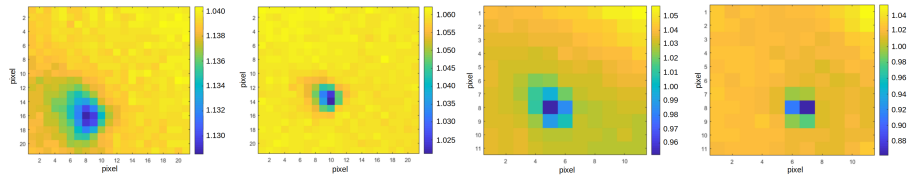

(a) No binning (b) 2×2 binning (c) 4×4 binning (d) 8×8 binning

Fig. 2. Spatial variarion of the NRF in the balanced case, obtained at different values of pixel binning. The lowest values are the following: a) $\sigma = 1.129 \pm 0.008$ in the case of no binning; b) $\sigma = 1.021 \pm 0.027$ for 2×2 binning; c) $\sigma = 0.952 \pm 0.044$ for 4×4 binning; d) $\sigma = 0.851 \pm 0.017$ for 8×8 binning.

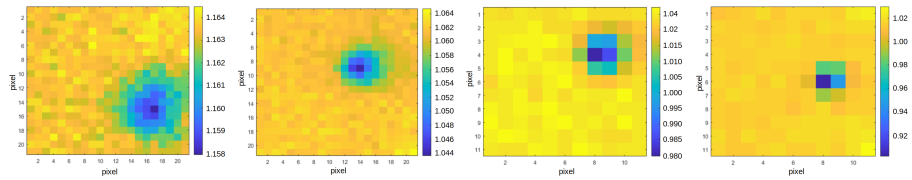

(a) No binning (b) 2×2 binning (c) 4×4 binning (d) 8×8 binning

Fig. 3. Spatial variarion of the NRF in the unbalanced case, obtained at different values of pixel binning. The lowest values are the following: a) $\sigma = 1.159 \pm 0.003$ in the case of no binning; b) $\sigma = 1.021 \pm 0.083$ for 2×2 binning; c) $\sigma = 0.980 \pm 0.020$ for 4×4 binning; d) $\sigma = 0.903 \pm 0.036$ for 8×8 binning.

(4) the procedure is repeated for each pixel belonging to an area $m \times m$ to which P belongs;
(5) an average among all the matrices obtained is calculated.

Fig. 2 reports the results in the balanced case, in which L_{3A} and L_{3B} at the same distance from L_2, while Fig. 3 reports the results in the unbalanced case; in both cases, the NRF has been evaluated for different pixel binnings.

The values reported in the captions of Figs. 2-3 refers to the NRF of the pixel with highest correlation. As expected, a binning (performed via hardware in our experiment) is required to obtain a value below 1. In particular, it takes at least a 4×4 binning, being $4\delta_p \sim w_0^s$. Note that, outside the correlation dip, the value of the NRF are close to unit (yellow background), as expected by two uncorrelated near-to-Poissonian photon number distributions which correspond to uncorrelated portions of the signal and idler beams. This confirms that the system is correctly calibrated. It is worth remarking the result in Fig. 3: the value of NRF can be kept smaller than 1, within the uncertainty, also in the unbalanced case, demonstrating the capability of this system to obtain sub shot-noise in a configuration in which CPI can be performed.

4. Conclusions and outlook

We have demonstrated the possibility to obtain a nonclassical noise-reduction factor, a necessary condition for sub-shot-noise imaging, in a setup in which Correlation Plenoptic Imaging can be effectively applied. Besides the obvious task of designing a new refocusing and 3D-reconstruction algorithm that works in the described setup, the most relevant step to be made in the following in order to efficiently incorporate the benefits of SSN imaging in CPI will be the definition of new correlation measurement methods, in which noise subtraction plays a relevant role. Examples of such algorithms are currently given by the differential ghost imaging protocols[27,28].

Acknowledgments

This work was supported by Istituto Nazionale di Fisica Nucleare (INFN) project "PICS – Plenoptic Imaging with Correlations", by PON ARS 01_00141 "CLOSE – Close to Earth" of Ministero dell'Istruzione, dell'Università e della Ricerca (MIUR), and through the EMPIR project 17FUN01-BeCOMe (EMPIR initiative is funded by the European Union Horizon 2020 research and innovation programme and cofinanced by the EMPIR participating States).

References

1. T. B. Pittman, Y. H. Shih, D. V. Strekalov, and A. V. Sergienko, *Phys. Rev. A* **52** (1995) R3429.
2. M. Genovese, *J. Opt.* **18** (2016) 073002.
3. O. Schwartz, J. M. Levitt, R. Tenne, S. Itzhakov, Z. Deutsch, and D. Oron, *Nano Lett.* **13** (2013) 5832.
4. Y. Israel, R. Tenne, D. Oron and Y. Silberberg, *Nat. Commun.* **8** (2017) 14786.
5. T. Dertinger, R. Colyer, G. Iyer, S. Weiss, J. Enderlein, *PNAS* **106** (2009) 22287.
6. G. Barreto Lemos, V. Borish, G. D. Cole, S. Ramelow, R. Lapkiewicz, and A. Zeilinger, *Nature* **512** (2014) 409.
7. M. D'Angelo, Y.H. Kim, S. P. Kulik, and Y. Shih, *Phys. Rev. Lett.* **92** (2004) 233601.
8. G. Scarcelli, Y. Zhou, and Y. Shih, *Eur. Phys. J. D* **44** (2007) 167.
9. F. Di Lena, F. V. Pepe, A. Garuccio, and M. D'Angelo, *Appl. Sci.* **8** (2018) 1958.
10. A. N. Boto, P. Kok, D. S. Abrams, S. L. Braunstein, C. P. Williams, and J. P. Dowling, *Phys. Rev. Lett.* **85** (2000) 2733.
11. D. Gatto Monticone, K. Katamadze, P. Traina, E. Moreva, J. Forneris, I. Ruo-Berchera, P. Olivero, I. P. Degiovanni, G. Brida, and M. Genovese, *Phys. Rev. Lett.* **113** (2014) 143602.
12. G. Brida, M. Genovese, and I. Ruo-Berchera, *Nat. Photonics* **4** (2010) 227.
13. I. R. Berchera and I. P. Degiovanni, *Metrologia* **56** (2019) 024001.
14. N. Samantaray, I. Ruo-Berchera, A. Meda, and M. Genovese, *Light Sci. Appl.* **6** (2017) e17005.
15. R. Hanbury Brown, R. Q. Twiss, *Proc. R. Soc. A* **242** (1957) 300.
16. R. Hanbury Brown, R. Q. Twiss, *Proc. R. Soc. A* **243** (1957) 291.
17. A. Gatti, E. Brambilla, M. Bache, and L. A. Lugiato, *Phys. Rev. Lett.* **93** (2004) 093602.
18. A. Valencia, G. Scarcelli, M. D'Angelo, and Y. Shih, *Phys. Rev. Lett.* **94** (2005) 063601.

19. G. Scarcelli, V. Berardi, and Y. Shih, *Phys. Rev. Lett.* **96** (2006) 063602.
20. M. D'Angelo, F. V. Pepe, A. Garuccio, and G. Scarcelli, "Correlation Plenoptic Imaging," Physical Review Letters **116**, 223602 (2016).
21. F. V. Pepe, F. Di Lena, A. Garuccio, G. Scarcelli, and M. D'Angelo, "Correlation plenoptic imaging with entangled photons," Technologies **4**, 17 (2016).
22. F. V. Pepe, O. Vaccarelli, A. Garuccio, G. Scarcelli, and M. D'Angelo, "Exploring plenoptic properties of correlation imaging with chaotic light", J. Opt. **19**, 114001 (2017).
23. G. Scala, M. D'Angelo, A. Garuccio, S. Pascazio, and F. V. Pepe, "Signal-to-noise properties of correlation plenoptic imaging with chaotic light," Phys. Rev. A **99**, 053808 (2019).
24. F. V. Pepe, F. Di Lena, A. Mazzilli, E. Edrei, A. Garuccio, G. Scarcelli, and M. D'Angelo, "Diffraction-Limited Plenoptic Imaging with Correlated Light," Phys. Rev. Lett. **119**, 243602 (2017).
25. L. Mandel, E. Wolf, *Optical Coherence and Quantum Optics* (Cambridge University Press, Cambridge, 1995).
26. A. Meda, E. Losero, N. Samantaray, F. Scafirimuto, S. Pradyumna, A. Avella, I. Ruo-Berchera, and M. Genovese, *J. Optics* **19** (2017) 094002.
27. F. Ferri, D. Magatti, L. A. Lugiato, and A. Gatti, *Phys. Rev. Lett.* **104** (2010) 253603.
28. E. Losero, I. Ruo Berchera, A. Meda, A. Avella, O. Sambataro, and M. Genovese, *Quantum differential ghost microscopy*, arXiv:1903.12630 (2019).